Bull. Mater. Sci. (2018) 41:77
https://doi.org/10.1007/s12034-018-1590-6

Synthesis and characterization of calcium-doped lanthanum manganite nanowires as a photocatalyst for degradation of methylene blue solution under visible light irradiation

A ARABI[1], M FAZLI[1,*] and M H EHSANI[2]
[1]Department of Chemistry, Semnan University, Semnan 35195-363, Iran
[2]Faculty of Physics, Semnan University, Semnan 35195-363, Iran
*Author for correspondence (mfazli@semnan.ac.ir)

MS received 22 July 2017; accepted 5 October 2017; published online 21 May 2018

Abstract. Calcium-doped lanthanum manganite (LCMO) powder was synthesized via hydrothermal method. The structural, morphological and optical properties of the resulting powder was characterized by X-ray diffraction (XRD), Fourier transform infrared spectroscopy (FTIR), inductively coupled plasma–atomic emission spectroscopy (ICP–AES spectrometer), field emission scanning electron microscopy (FESEM) and UV–Vis spectroscopy (UV–Vis). The XRD results showed the existence of only one crystalline phase. FESEM image indicates that the LCMO sample has nanowire structure with an average diameter of ∼125 nm. The band gap energy of the sample was about 2.13 eV. The as-prepared nanowires showed sufficient visible-light photocatalytic activity for the water treatment from dyes and toxic organic materials. The photodegradation efficiency for decolourizing methylene blue solution (7 ppm) by LCMO nanowires ($0.07\,g\,l^{-1}$), after 360 min illumination, was about 73% with a reaction rate constant of $0.003\,min^{-1}$. The six times cycled results suggested the great long-term stability of the photocatalyst.

Keywords. Nanowires; hydrothermal method; photocatalyst; methylene blue.

1. Introduction

The perovskite-type manganites were considered as a one of the most interesting materials recently because of their chemical and physical properties. These materials have general formula ABO_3, in which A is La, Ca, Ba, Sr, Na, K ion and B is Mn, Fe, Ti, Co, Ni, Cr ion [1–3]. Sun *et al* [4] reported that the physical and chemical activities of these materials are due to two main factors: (1) corner-shared BO_6 octahedron network in its unit cell, which can facilitate electron hopping. This makes ABO_3 compound as a superior catalyst for the degradation of pollutant by inducing high reducibility. (2) The atoms at A-site of ABO_3 help the stabilization of multiple valence states of B site cations. This will make the electrons of ABO_3 oxides more active, so that they can be excited easily by the external factor such as light irradiation. The presence of alkaline earth metal substituent in the A site decreases the band gap energy and changes the magnetic, electric and photocatalytic properties.

In this type of perovskite oxides, the doped lanthanum-based $La_{1-x}A_xMnO_3$ manganites (A is an alkaline element such as Ca^{2+}, Sr^{2+}, Na^+, K^+, etc.) have interesting properties. These materials have mixtures of Mn^{3+} and Mn^{4+} ions that play a major role in their properties. This substitution modifies the structure by rotating the MnO_6 octahedral as well as changing the Mn–O–Mn bond length and angle. Many theories like the Jahn Teller (JT) distortion and the double exchange (DE) mechanism are introduced to explain this phenomenon [5]. The properties of $La_{1-x}A_xMnO_3$ perovskite-type oxides are related to their stoichiometry and degree of substitution of the alkaline element for La [6]. $La_{1-x}Ca_xMnO_3$ is a mixed valence manganese oxide or doped manganese perovskite family, which widely used in many applications. In this present work, we have investigated the synthesis of the pure $La_{1-x}Ca_xMnO_3 (x \approx 0.3)$ nanowires by hydrothermal method and its photocatalytic activity was examined under visible light irradiation at room temperature.

Photocatalysis is a process by which a semiconductor material absorbs energy of irradiation equal or greater than to its band gap energy. It can excite the electrons from valence band to conduction band. Such a charge hopping leads to the formation of electron–hole pairs, which can further generate free radicals in the system for redox of the substrate. The resulting free-radicals are very efficient oxidizers of organic materials which can degrade organic pollutants [7–9]. The use of visible light semiconductor photocatalysts has recently attracted much attention [10–12], since this process does not require additional chemicals and the main component is the solar spectra and indoor illuminations [13,14]. In recent years, the photocatalytic activity of perovskite-type oxides has received considerable attention due to its high catalytic activity, low cost and environmental adaptability [15–17]. To the best of our knowledge, this is the first study of its kind that

reports the utility of $La_{1-x}Ca_xMnO_3 (x \approx 0.3)$ nanowires in photodegradation process.

2. Methods

2.1 *Chemicals and materials*

Analytical grade $KMnO_4$, $MnCl_2 \cdot 4H_2O$, $La(NO_3)_3 \cdot 4H_2O$, $Ca(NO_3)_2 \cdot 4H_2O$ and KOH were purchased from Merck Company and used without any purification. KOH served as a mineralizer.

2.2 *Synthesis of calcium-doped manganite nanowires*

The molar ratios of La/Ca/Mn were kept at 0.7/0.3/1 based on the stoichiometric ratio of $La_{0.7}Ca_{0.3}MnO_3$ amounts.

The initial molar ratios for the synthesis of nominal composition $La_{0.7}Ca_{0.3}MnO_3$ were $3KMnO_4$:$0.7MnCl_2 \cdot 4H_2O$:$0.7 La(NO_3)_3 \cdot 6H_2O$:$0.3Ca(NO_3)_2 \cdot 4H_2O$:$606KOH$:$1682H_2O$. The initial mole ratio of the manganese salts was calculated based on valences of the reactants to obtain the desired average manganese oxidation state of 4^+ in the reaction mixture. The typical synthesis of LCMO nanowires procedure is as follows. The KOH solution was added as a mineralizer to adjust the pH of the solution to 14. The synthesis of calcium-doped lanthanum manganite by hydrothermal method was performed by mixing fresh solutions of $KMnO_4$, $MnCl_2$, $Ca(NO_3)_2$ and $La(NO_3)_3$ prepared in deionized water in appropriate concentrations. The solutions of $La(NO_3)_3$, $Ca(NO_3)_2$ and $MnCl_2$ were added respectively into a 100 ml glass container with lid and stirred using a magnetic bar and then, KOH solution was added to the resulting homogeneous solution. Finally, the $KMnO_4$ solution was added to the solution containing Mn^{2+}, La^{3+} and Ca^{2+} cations. Immediately after MnO_4^- addition, precipitation of insoluble Mn^{4+} containing dark-brown oxides can be observed. The as-prepared reaction mixture was stirred vigorously for 30 min to obtain a homogeneous black solution and then poured into a 200 ml Teflon vessel till 55% of its volume was filled and then, the vessel was sealed in a stainless steel autoclave for hydrothermal treatment. The crystallization was performed at 170°C under autogenous pressure for 48 h. After the autoclave was cooled to room temperature naturally and depressurized, the final product was separated, washed with deionized water and dried in ambient air at 120°C overnight. In the final process, the obtained powder was heat-treated at 800°C and 6 h. The detailed reaction conditions and corresponding brief results are summarized in figure 1.

The structural, spectroscopic and optical characterizations of the resulted powders were systematically characterized by X-ray diffraction (XRD), inductively coupled plasma–atomic emission spectroscopy (ICP–AES), field emission scanning electron microscopy (FESEM), Fourier transform infrared spectroscopy (FTIR) and UV–Vis absorption spectroscopy. The photocatalytic activity of the as-prepared nanostructures was examined using the photodegradation of aqueous methylene blue (MB) solution as a model of pollutant under visible light irradiation at room temperature.

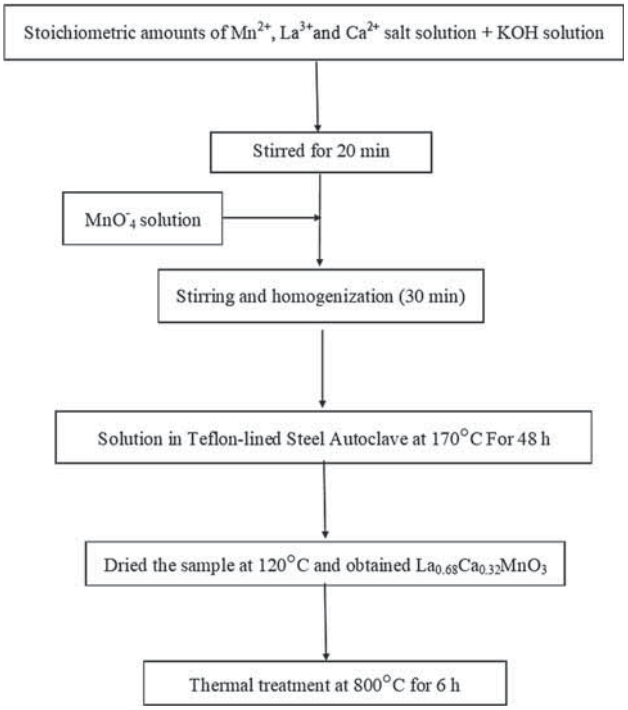

Figure 1. Flowchart of synthesis of LCMO sample.

2.3 *Photocatalytic measurements and sample preparation*

Photocatalytic degradation of MB as a usual resistant dye to biodegradation was used as a probe reaction to investigate photocatalytic activity of LCMO nanowires.

The photocatalytic degradation of aqueous MB solution (7 ppm and pH = 4) by LCMO as photocatalyst ($0.07 g\,l^{-1}$) was carried out in a 100 ml glass beaker at 25°C under magnetic stirring and irradiation of three 40 W fluorescent lamps ($25 mW\,cm^{-2}$) as a visible-light source.

At first, the mixture of water and photocatalyst was ultrasonicated for 10 min. Then, MB solution was added properly with a magnetic stirrer during the photocatalysis process and pH was constant along the photodegradation reaction. The pH of solution has a main part in the photodegradation processes of water treatment, which influences the surface-charge properties of the catalysts. The changes in pH upon photodegradation of the MB were studied and the best result was obtained in pH of 4. Dye solutions of about 3 ml were taken out at regular intervals and the dispersed photocatalyst was removed by centrifugation and the absorbance of remaining MB solution was measured. The decreasing concentration of MB in the solution was used to investigate the activity of the LCMO nanowires. The characteristic absorption peak of MB solution at 665 nm was chosen as the monitored parameter to detect the concentration of MB solution. The controlling experiments were also carried out under visible light without

photocatalyst and in the dark with photocatalyst. The result showed that aqueous MB solution does not undergo photodegradation under visible light irradiation. Before illumination, the mixture was magnetically stirred in the dark for 15 min to ensure adsorption–desorption equilibrium of the MB onto the surface of the photocatalyst. The amount of photodegradation was controlled by monitoring the absorbance characteristic of the MB, which was proportional to its concentration in the solution.

2.4 *Structural and spectroscopic characterization*

Thermogravimetric analysis (TGA) of the dried sample and its phase formation were characterized using a STA PT 1600, LINSEIS instrument (Germany). The experiment was carried out under atmosphere at a heating rate of 5°C min^{-1} up to 1000°C. The XRD patterns of heat-treatment powder at 800°C and 6 h were recorded by using a Philips PW 1710 X-ray diffractometer with CuK α radiation ($\lambda = 0.15418$ nm). The XRD patterns were collected in a 2θ range of 20−80° degree at room temperature, with a 2θ step size of 0.05° and a time per step of 5 s. Rietveld refinement was performed with the FULLPROF software for the diffraction peak shape.

The morphology and size distribution of the sample were examined by Mira 3-XMU FESEM and images elaborated with Image software (Digimizer software). The chemical compositions of metal elements in the sample were measured by ICP–AES spectrometer, Spectro Genesis metek (Germany). The FTIR was recorded on an FTIR 8400 S, Shimadzu (Japan) spectrophotometer in the region of 4000–400 cm^{-1} with a scan resolution of 2 cm^{-1} using KBr pellets. Electronic absorption spectra were recorded on a UV-165 PC, Shimadzu (Japan) double-beam spectrophotometer.

3. Results and discussion

3.1 *Synthesis and structural characterization*

Figure 2 shows the TGA curve of the as-prepared sample at heating rates of 5°C min^{-1} from 25 to 1000°C. The result of TGA analysis could be used to estimate the calcination temperature. According to the discussion of TGA results by Sujittra *et al* [18], relatively similar results were also obtained for the preparation of perovskite phases with doping by Ca cations. The curve shows that weight loss has occurred in several steps. The first step is weight loss (25%) below 330°C, mostly due to loss of water, which can be attributed to dehydration of the water. The second is decomposition step begins at 330°C and ends at 640°C, attributed to the decomposition of $La(NO_3)_3$, $Ca(NO_3)_2$, $KMnO_4$, $MnCl_2$ and KOH into $La(OH)_3$, LaOOH, $Ca(OH)_2$ and MnO_2 in air. The third step is thermal decomposition begins at 640°C and ends at 780°C, attributed to the decomposition of $La(OH)_3$, LaOOH and MnO_2 into $La_{0.7}Ca_{0.3}MnO_3$ in air. A very weak weight loss on the TGA curves was recognized in the range of 780–820°C.

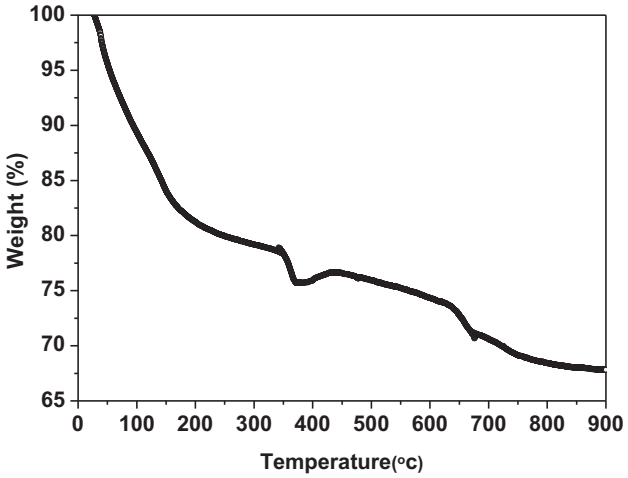

Figure 2. TGA measurement for the hydrothermally obtained powder.

It can be assigned to the decomposition of intermediate materials and the formation of perovskite phase. The perovskite oxide phase formation appears to occur at a temperature of ∼650°C and completes at 800°C. This assumption will be further investigated and again confirmed by XRD analyses [19,20].

The as-prepared sample was ground and then heat-treated at 800°C for 6 h with regard to TGA results. The material obtained after this treatment was a semiconductor material.

The XRD pattern of calcined sample was successfully indexed in the orthorhombic perovskite structure within the Pnma space group. For the sample heat-treated at 800°C, no signal from secondary phase was detected and showed a well-crystallized perovskite-type structure. The structural parameters of sample were refined with the FULLPROF software. The Rietveld refinement was used to determine the lattice parameters, bond length and bond angles between Mn and O in the octahedral cage (MnO_6) in the perovskite structure by fitting the obtained XRD pattern with a crystal model from mathematical approximation. Both the experimental and refined XRD patterns are shown in figure 3. The structural parameters and fit factor values, which are in line with the previously reported values [21–23] are listed in table 1.

FTIR spectrum of the sample is shown in figure 4. Two absorption bands around 600 and 400 cm^{-1} were observed for the composition. The higher frequency band at 585 cm^{-1} corresponds to the stretching mode (ν_s) of Mn–O–Mn or Mn–O bonds, which involves the internal motion of a change in Mn–O bond length [24,25], while the band around 400 cm^{-1} corresponds to the bending mode (ν_b), which is due to a change in the Mn–O–Mn bond angle. These two bands are related to the environment surrounding the MnO_6 octahedra in the ABO_3 perovskite and confirms the formation of perovskite structure, which is in agreement with the XRD results [26,27]. Small difference in ν_s and ν_b values related to changes in the Mn–O–Mn bond length and angle, which were obtained

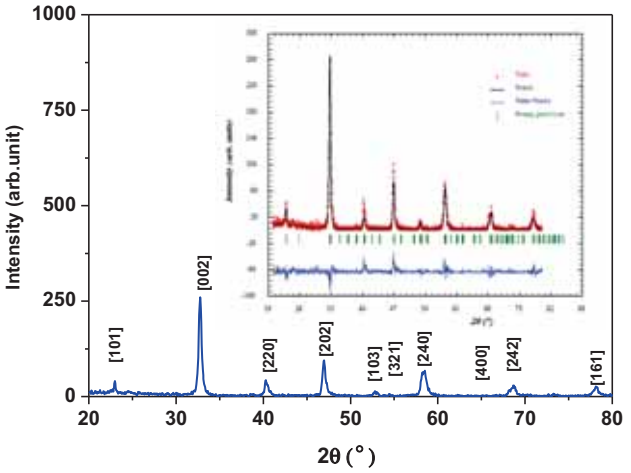

Figure 3. Room temperature XRD pattern of the sample. Inset: room temperature XRD pattern (red symbol) and Rietveld profile file (black line).

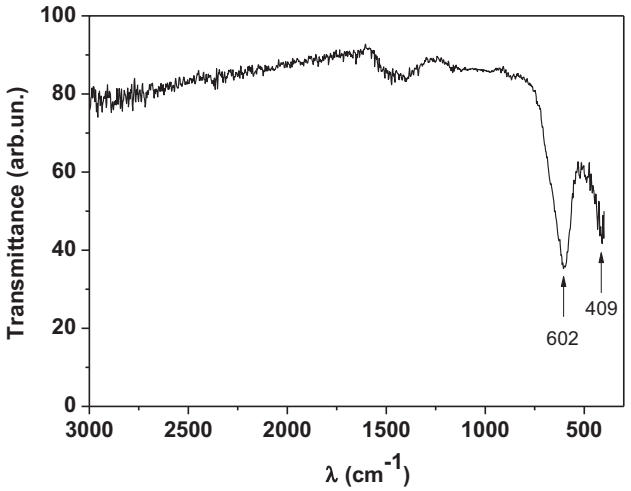

Figure 4. FTIR spectrum of synthesized sample.

using structural refinement (table 1). The extra peaks in the FTIR spectra related to $KBr(H_2O)_n$ and CO_2 corresponding to the wavenumbers of about 1550 and 2350 cm^{-1} exist in ambient conditions.

The chemical compositions of metal elements in the samples were measured by ICP–AES. The data obtained from ICP analyses are given in table 2. From the data collected in table 2, composition of sample is close to the stoichiometric of nominal composition $La_{0.7}Ca_{0.3}MnO_3$ and it is named as $La_{0.68}Ca_{0.32}MnO_3$.

The morphological image of synthesized sample was studied by FESEM technique. Figure 5 indicates that the sample consists of uniform distribution of monodisperse nanowires with typical lengths in the range of several to several tens of micrometres.

The Digimizer software was used to determine the mean diameter size of the wires on the SEM images. The inset in figure 5 shows the dispersion histogram. The results showed mean diameter size equal to 126.8 nm by the standard deviation of 40.2 nm [28]. It is evident that the morphology of as-prepared sample under our condition is quite different from that reported by others [18,22,23,29].

It is interesting that the orthorhombic-structured manganites can grow in the nanowire form, which probably indicates the presence of uniaxial nucleation centres in the hydrothermal method [30]. The factors such as manganese and metal precursors, ultrasonic treatment and hydrothermal conditions (e.g., temperature, time and pH value), concentration of mineralizer and the mechanism of crystal growth could have an effect on the morphology of the as-synthesized products [23,31,32].

Considering the potential opto-catalytic applications for LCMO in photodegradation processes, the optical absorption spectrum was obtained. Figure 6 indicates the UV–Vis optical absorption spectra of the synthesized specimen. The semiconductors with ultra violet band gap are less suitable for visible light photodegradation compared with that of visible band gap semiconductors. Various approaches were investigated in the past to reduce band gap of UV-active semiconductors to overlap with the solar spectrum. A parent compound, $LaMnO_3$, has an antiferromagnetic insulating ground state with four 3d electrons in a high spin configuration, i.e., $t_2g^3eg^1$. By substituting La with a divalent cation, Mn^{4+} ions can be introduced [33]. Thus $La_{1-x}Ca_xMnO_3$ compounds belong to the hole-doped manganite perovskites. Since the parent sample ($LaMnO_3$) is Mn^{3+}-rich, $La_{1-x}Ca_xMnO_3$ ($La^{3+}_{1-x}Ca^{2+}_xMn^{3+}_{1-x}Mn^{4+}_xO_3$) with mixed-valence Mn^{3+} and Mn^{4+} plays a major role in the electronic structure of this sample.

In the cubic lattice environment, Mn-site settle at the centre and surrounded by six oxygen atoms forming an octahedral structure and La/Ca cations at the corners of the cube.

The five Mn-3d orbitals split into low lying narrower t_{2g} triplet and high-lying broader e_g doublet sub-bands by the crystal field (CF) energy. Each of these e_g sub-bands is further split into up- and down-spin bands due to the exchange interaction. The two-fold degenerate e_g levels (e_{1g} and e_{2g})

Table 1. Structural parameters obtained by Rietveld refinement method.

a (Å)	*b* (Å)	*c* (Å)	*V* (Å^3)	GOF	d_{Mn-O} (Å)	θ_{Mn-O} (°)	*D* (nm)
5.4548	7.7552	5.4887	232.1888	1.055	1.947	169.48	23.02

Table 2. The stretching mode, bending mode and ICP results of the sample.

Nominal composition	ν_s (cm^{-1})	ν_b (cm^{-1})	ICP results La:Ca:Mn	La/(La + Ca) ratio	Ca/(La + Ca) ratio	Composition
$La_{0.7}Ca_{0.3}MnO_3$	602	409	0.721:0.348:1.04	0.68	0.32	$La_{0.68}Ca_{0.32}MnO_3$

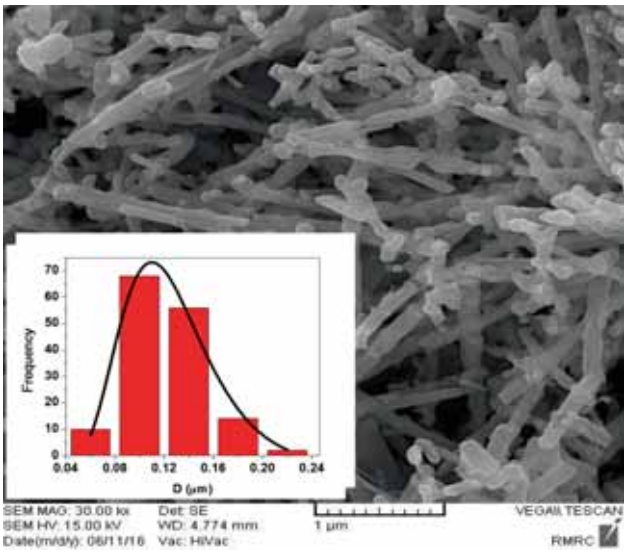

Figure 5. Scanning electron microscopy image of a sample. Inset: dispersion histogram of particles.

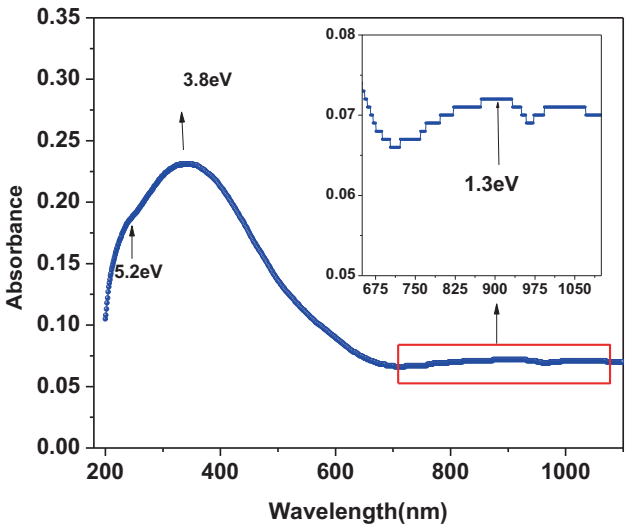

Figure 6. Room-temperature UV–Vis spectra of the nanowires.

are empty in the Mn^{4+} ion and occupied by one electron with spin parallel to the core spin in the Mn^{3+} ion. There are several charge transfer transitions such as the transitions $Mn^{3+}(e_{1g}) \rightarrow Mn^{3+}(e_{2g})$, $Mn^{3+}(e_{1g}) \rightarrow Mn^{4+}(e_g)$, $O^{2-}(2p) \rightarrow Mn^{3+}(e_{2g})$, $O^{2-}(2p) \rightarrow Mn^{4+}(e_g)$, in the $La_{0.7}Ca_{0.3}MO_3$ manganites. Meanwhile, some physical rules

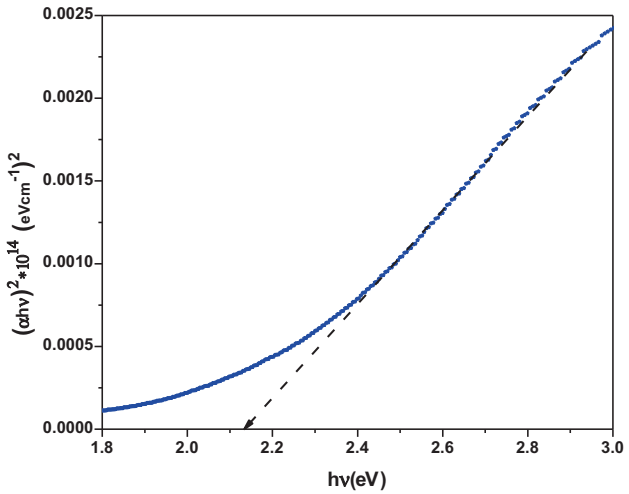

Figure 7. The plot of $(\alpha h\nu)^2$ *vs.* photon energy ($h\nu$) of the $La_{0.68}Ca_{0.32}MnO_3$ nanowires.

such as parity and spin polarity forbid charge transfer citations in $t_{2g} \rightarrow e_g$ and $e_g \rightarrow e_g$. These transitions may be allowed by spin–orbit coupling, lattice distortions/disorder and mixing of odd parity wavefunctions [34]. In figure 6, three obvious peaks are observable due to optical response in the sample. First peak is observed around 235 nm (5.2 eV), strong absorption peak is observed at wavelengths about 325–380 nm (3.8–3.3 eV) and the third peak occurs as shown in the inset of figure 6 around 950 nm (1.3 eV) for the sample.

The band gap energy of the LCMO nanoparticles evaluated from the UV–Vis spectra by Tauc's plot of $(h\nu\alpha)^2$ *vs.* ($h\nu$) and extrapolation of the linear portions of the curve to the energy axis according to the following equation [7,15,35]:

$$(\alpha h\nu)^2 = A(h\nu - E_g), \tag{1}$$

where α is the absorption coefficient, E_g the band gap energy, $h\upsilon$ the photon energy and A the constant dependant on the effective masses of the electron, the hole, and the material refractive index. The Tauc's plot of the sample is shown in figure 7. The estimated optical band gap of $La_{0.68}Ca_{0.32}MnO_3$ nanowires is about 2.13 eV.

3.2 *Photocatalytic properties of Ca-doped manganite nanowires*

The photocatalytic degradation of MB dye in aqueous solution was performed using the as-prepared LCMO sample

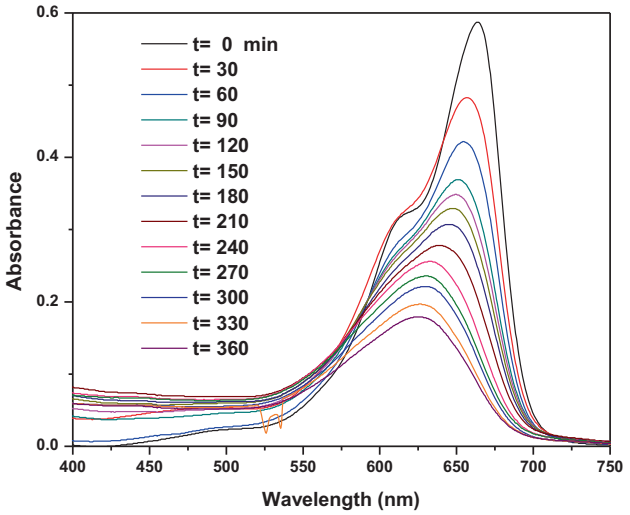

Figure 8. Absorption spectral changes and photodegradation of aqueous methylene blue (MB) solution degraded by $La_{0.68}Ca_{0.32}MnO_3$ nanowires under visible light.

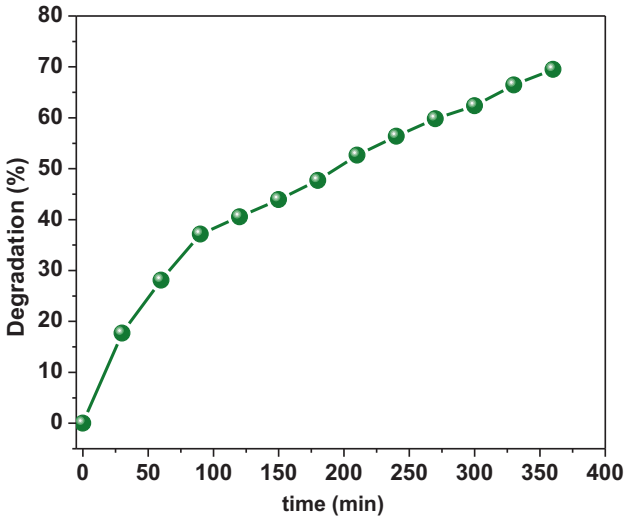

Figure 9. Degradation percent of methylene blue in the presence of $La_{0.68}Ca_{0.32}MnO_3$ photocatalyst under visible light irradiation.

as a photocatalyst under ordinary visible light. The initial concentration of MB solution was fixed based on similar studies conducted by researchers [36,37]. Three 40W fluorescent lamps were used as the visible light source and kept 5 cm above and around the MB solution surface. Some important matters for photocatalytic treatment of water are to define characteristics of the water to be treated in terms of water composition and pH [13,38]. The effect of pH on the degradation of MB was studied and the highest efficiency of photodecomposition process was obtained at pH 5. Figure 8 shows photodegradation of MB solution (7 ppm) using the sample (0.07 g l^{-1}) after irradiation under visible light at different time intervals (0–360 min). The UV–Vis spectra of MB solution showed gradual degradation of MB with increase in time. The maximum absorption peak of MB at 665 nm continuously decays with illumination time, along with a change in the blue colour solution from deep to light.

The degradation percent of MB [1,15,36,37] were evaluated by equation (2):

$$D\% = (A_0 - A)/A_0 \times 100, \tag{2}$$

where A_0 is the initial absorbance of MB solution and A the absorbance of MB solution after degradation.

Figure 9 shows that the 0.070 g l^{-1} of photocatalyst degrades MB solution (7 ppm) up to 70% in 360 min.

When the reaction mixture is stirred for 30 min without light illumination, a slight decrease in the MB concentration is not noticed. This decrease in MB concentration originates from adsorption of MB by the catalyst because of its surface hydrophilicity.

The kinetic behaviour between the MB molecules and the photocatalyst could be presented by Langmuir–Hinshelwood model [9,12,15,38–41]. This model was used for heterogeneous photocatalytic degradation to determine the relationship between the apparent first-order reaction rate constant and the initial content of the organic substrate. Figure 10 shows that the degradation of MB follows the pseudo first-order kinetics expressed as equation (3):

$$r = -(\mathrm{d}C/\mathrm{d}t) = K_{\mathrm{app}}C, \tag{3}$$

where K_{app} is the apparent first-order reaction rate constant and it is the reaction time. Integrating of this equation (with the restriction $C = C_0$ at $t = 0$ with C_0 being the initial concentration in the bulk solution in dark adsorption) will lead to equation (4):

$$-\ln(C_t/C_0) = K_{\mathrm{app}}t, \tag{4}$$

where C_0 is the initial concentration of MB and C_t the concentration of MB at the reaction time t.

The slope of the linear plot in figure 10 is equal to apparent first-order reaction rate constant (K_{app}). So, this obtained value was 0.003 min^{-1} in the presence of the synthesized photocatalyst.

3.3 *Photocatalyst reusability*

The stability performance and reusability of photocatalysts are important parameters from the point of view of economical and practical applications [13,42]. The reusability of the synthesized sample was investigated by recycling the solid sample that covered by MB molecules after the photocatalytic degradation under visible-light irradiation. The photocatalysts were collected after each run and washed with 0.01 M H_2SO_4 solution and a sufficient amount of deionized water,

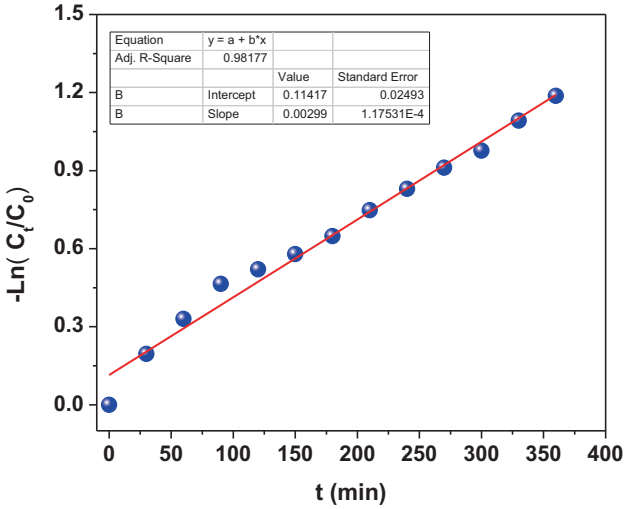

Figure 10. Pseudo-first-order kinetics plot of methylene blue degradation over $La_{0.68}Ca_{0.32}MnO_3$ nanophotocatalyst.

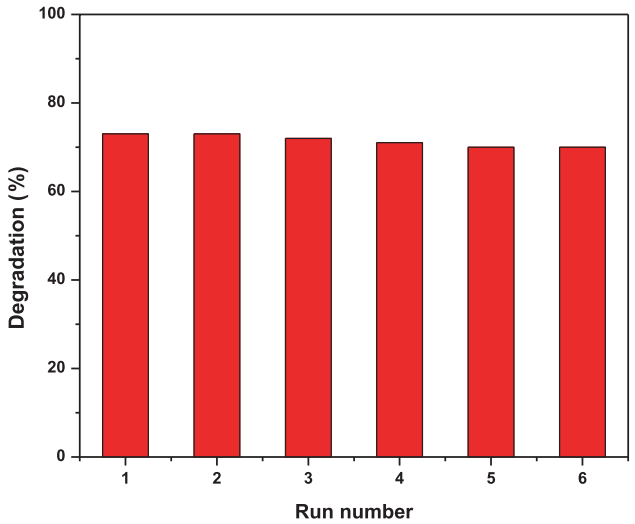

Figure 11. Reusability of the prepared sample.

respectively. In each run, the photocatalytic activity of the solid sample was performed in the same condition as mentioned before and shown in figure 11. The results show that this material can retain its photocatalytic activity for at least six reaction cycles.

3.4 *Photocatalysis mechanism*

When an aqueous solution consist of photocatalyst, air or oxygen, and MB as organic contaminant irradiated under UV or visible light ($h\upsilon$), then electron–hole pairs would be produced (equation (5)). These photogenerated electron–hole pairs are powerful reducing and oxidizing agents, respectively. The generated holes in the valence band react with OH^- or H_2O, which were adsorbed on the surface of photocatalyst to give the hydroxyl radical ($^\bullet OH$) (equation (6)). The produced hydroxyl radicals react with MB molecules and produce various materials such as carbon dioxide, water, nitrate, sulphate and hydrochloric acid at very low concentrations (equation (7)) [8,40,41]. The excited electrons in the conduction band react with O_2, which were adsorbed on the surface of photocatalyst to form superoxide radical ion ($^\bullet O_2^-$) (equation (8)). The photoreaction process is shown in scheme 1.

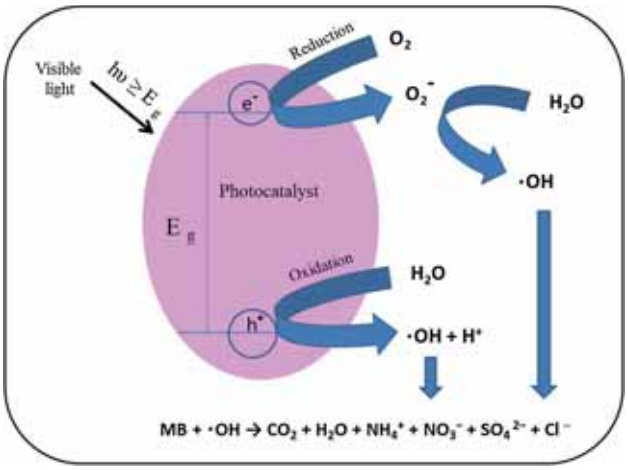

Scheme 1. A schematic diagram of the charge transfer process for the $La_{0.68}Ca_{0.32}MnO_3$ nanowires photocatalytic degradation of methylene blue.

$$La_{0.68}Ca_{0.32}MnO_3 + h\upsilon \rightarrow La_{0.68}Ca_{0.32}MnO_3(h^+_{VB} + e^-_{CB}), \quad (5)$$

$$La_{0.68}Ca_{0.32}MnO_3(h^+_{VB}) + OH^- \rightarrow La_{0.68}Ca_{0.32}MnO_3 + {}^\bullet OH, \quad (6)$$

$$MB + {}^\bullet OH \rightarrow CO_2 + H_2O + NH_4^+ + NO_3^- + SO_4^{2-} + Cl^-, \quad (7)$$

$$La_{0.68}Ca_{0.32}MnO_3(e^-_{CB}) + O_2 \rightarrow La_{0.68}Ca_{0.32}MnO_3 + {}^\bullet O_2^- \quad (8)$$

4. Conclusions

In this study, $La_{0.68}Ca_{0.32}MnO_3$ nanowires was synthesized by a simple hydrothermal method followed by heat treatment at 800°C. XRD results showed that obtained sample had perovskite structure. FESEM images showed micrometre-sized (0.05–0.22 μm) randomly distributed crystal nanowires. Using Tauc's equation, it was obtained that the product has a direct band gap value of 2.13 eV, which is in the range of effective photocatalytic activity at visible light irradiation.

The photocatalytic activity of the sample was investigated by degradation of MB in aqueous solution under visible-light irradiation. The results revealed that $La_{0.68}Ca_{0.32}MnO_3$ nanowires exhibited sufficient photocatalytic activity for degradation of MB solution under visible-light irradiation.

The photodegradation efficiency for decolourizing MB solution (7 ppm), by doped calcium lanthanum manganite ($0.07\,g\,l^{-1}$) after 360 min of illumination, was about 73% with a reaction rate of $3 \times 10^{-3}\,min^{-1}$.

References

[1] Bradha M, Vijayaraghavan T, Suriyaraj S P, Selvakumar R and Ashok A M 2015 *J. Rare Earth* **33** 160

[2] Yang Y, Sun Y and Jiang Y 2006 *Mater. Chem. Phys.* **96** 234

[3] Chen H X, Wei Z X, Wang Y, Zeng W W and Xiao C M 2011 *Mater. Chem. Phys.* **130** 1387

[4] Sun M, Jiang Y, Li F, Xia M, Xue B and Liu D 2010 *Mater. Trans.* **51** 1981

[5] Shaikh M W, Mansuri I, Dar M A and Varshney D 2015 *Mater. Sci. Semicond. Process* **35** 10

[6] Culebras M, Toran R, Gomez C M and Cantarero A 2014 *Nanoscale Res. Lett.* **9** 1

[7] Szabo-Bardos E, Somogyi K, Toro N, Kiss G and Horvath A 2011 *Appl. Catal. B Environ.* **101** 471

[8] Wang S, Yun J H, Luo B, Butburee T, Peerakiatkhajohn P, Thaweesak S *et al* 2017 *Mater. Sci. Technol. Ser.* **33** 1

[9] Eskandarian M R, Choi H, Fazli M and Rasoulifard M H 2016 *Chem. Eng. J.* **300** 414

[10] Yi Z, Ye J, Kikugawa N, Kako T, Ouyang S, Williams H S *et al* 2010 *Nat. Mater*. **9** 559

[11] Wei M, Wan J, Hu Z, Peng Z, Wang B and Wang H 2017 *Appl. Surf. Sci.* **391** 267

[12] Lorkit P, Panapoy M and Ksapabutr B 2014 *Energy Proc.* **56** 466

[13] Maleki M and Haghighi M 2016 *J. Mol. Catal. A Chem.* **424** 283

[14] Andrade G R S, Nascimento C C, Neves E C, Barbosa C D A E S, Costa L P, Barreto L S *et al* 2012 *J. Hazard. Mater.* **203–204** 151

[15] Shaterian M, Enhessari M, Rabbani D, Asghari M and Salavati-Niasari M 2014 *Appl. Surf. Sci.* **318** 213

[16] Fu S, Niu H, Tao Z, Song J, Mao C, Zhang S *et al* 2013 *J. Alloys Compd*. **576** 5

[17] Yang H, Zhang J X, Lin G J, Xian T and Jiang J L 2013 *Adv. Powder Technol*. **24** 242

[18] Sujittra D, Chunpen T, Charusporn M and Santi M 2012 *J. Supercond. Nov. Magn*. **25** 2507

[19] Soleymani M, Moheb A and Babakhani D 2011 *Chem. Eng. Technol*. **34** 49

[20] Wenwei W, Jinchao C, Xuehang W, Sen L, Kaituo W and Lin T 2013 *Adv. Powder Technol*. **24** 154

[21] Varshney D, Mansuri I, Kaurav N, Lung W Q and Kuo Y K 2012 *J. Magn. Magn. Mater*. **324** 3276

[22] Vertruyen B, Rulmont A, Cloots R, Fagnard J F, Ausloos M, Vandriessche I *et al* 2005 *J. Mater. Sci.* **40** 117

[23] Chihoub R, Amira A, Mahamdioua N, Altintas S P, Varilci A and Terzioglu C 2016 *Physica B* **492** 11

[24] Gao F, Lewis R A, Wang X L and Dou S X 2000 *Physica C* **341–348** 2235

[25] Nagabhushana B M, Chakradhar R P S, Ramesh K P, Shivakumara C and Chandrappa G T 2007 *Mater. Chem. Phys*. **102** 47

[26] Gao F, Lewis R A, Wang X L and Dou S X 2002 *J. Alloys Compd*. **347** 314

[27] Arulraj A and Rao C N R 1999 *J. Solid State Chem*. **145** 557

[28] Lavorato G C, Lima J E, Tobia D, Fiorani D, Troiani H E, Zysler R D *et al* 2014 *J. Nanotechnol.* **25** 355704

[29] Regaieg Y, Ayadi F, Monnier J, Reguer S, Koubaa M, Cheikhrouhou A *et al* 2014 *Mater. Res. Exp.* **1** 046105

[30] Teng F 2009 *Solid State Sci*. **11** 1643

[31] Deng J, Zhang L, Dai H, He H and Au C T 2009 *J. Mol. Catal. A Chem*. **299** 60

[32] Rizzuti A and Leonelli C 2009 *Process. Appl. Ceram*. **3** 29

[33] Choi S G, Lee H S, Choi H, Chung S W and Park H H 2013 *Thin Solid Films* **529** 352

[34] Cesaria M, Caricato A P, Leggieri G, Martino M and Maruccio G 2013 *Thin Solid Films* **545** 592

[35] Patra A S, Kumar N V, Barpuzary D, De M and Qureshi M 2014 *Mater. Lett.* **131** 125

[36] Chen M L and Oh W C 2011 *Nanoscale Res. Lett*. **6** 1

[37] Zhou F and Zhu Y 2012 *J. Adv. Ceram*. **1** 72

[38] Dariani R S, Esmaeili A, Mortezaali A and Dehghanpour S 2015 *Optik* **127** 7143

[39] Ghosh T, Ullah K, Nikam V, Park C Y, Meng Z D and Oh W C 2013 *Ultrason. Sonochem*. **20** 768

[40] Soltani N, Saion E, Hussein M Z, Erfani M, Abedini A, Bahmanrokh G *et al* 2012 *Int. J. Mol. Sci*. **13** 12242

[41] Xu X, Lu R, Zhao X, Xu S, Lei X, Zhang F *et al* 2011 *Appl. Catal. B* **102** 147

[42] Lv J, Li D, Dai K, Liang C, Lu L, Jiang D *et al* 2017 *Mater. Chem. Phys*. **186** 372